The Astrophysical Journal, 704:274–280, 2009 October 10 doi:10.1088/0004-637X/704/1/274

MOLECULAR HYDROGEN FORMATION CATALYZED BY POLYCYCLIC AROMATIC HYDROCARBONS IN THE INTERSTELLAR MEDIUM

Valéry Le Page[1,2], Theodore P. Snow[1,2], and Veronica M. Bierbaum[1,2]
[1] Center for Astrophysics and Space Astronomy, University of Colorado, Boulder CO 80309, USA
[2] Department of Chemistry and Biochemistry, University of Colorado, Boulder CO 80309, USA
Received 2008 December 11; accepted 2009 August 25; published 2009 September 22

ABSTRACT

We present an alternate model for the formation of molecular hydrogen in the interstellar medium (ISM) where polycyclic aromatic hydrocarbon (PAH) cations may play a key role as catalysts. The mechanism involves the chemical trapping of H atoms on the periphery of the PAH carbon skeleton and the subsequent release of H_2 through dissociative recombination of the hydrogenated ion with an electron. The estimated rate coefficient of H_2 production using this process compares well with a widely accepted value of 3×10^{-17} cm^3 s^{-1} for H_2 formation on grains in the diffuse ISM. It is inferred that PAHs can contribute significantly to the formation of molecular hydrogen, especially in environments where the classical process of H adsorption on grains is impeded by high UV fluxes as in diffuse clouds and photon-dominated regions.

Key words: astrochemistry – molecular processes

1. INTRODUCTION

The role of the hydrogen molecule is central to astrophysics; as a cooling agent it triggers the collapse of molecular clouds which lead to star formation, and as a molecular agent it is a major contributor to the chemical processes which lead to the synthesis of complex polyatomic molecules in clouds.

Although H_2 is the most abundant molecular species in the universe, its detailed mechanism of formation still remains an open problem. Since the pioneering work of Gould & Salpeter (1963) 45 years ago it is believed that H_2 molecules form on grains. Two mechanisms have been proposed: the Langmuir–Hinshelwood mechanism where H atoms migrate from one adsorption site to another, followed by an encounter with another adsorbed H atom and the subsequent release of an H_2 molecule; and the Eley–Rideal mechanism where the incoming H atom directly recombines with another H atom trapped on an adsorption site.

The hypothesis of H_2 formation on grains originates from the failure of gas-phase models to produce an efficient H_2 formation network (Duley & Williams 1984). Any pure gas-phase model of H_2 formation suffers from the poor efficiency of radiative association between small molecules or atoms. For example, in the case of $H^- + H \rightarrow H_2 + e^-$ or $H_2^+ + H \rightarrow H_2 + H^+$, which are potentially efficient routes for molecular hydrogen formation, the overall process is inefficient because it relies on one of two prior radiative association reactions, $H + e^- \rightarrow H^-$ or $H + H^+ \rightarrow H_2^+$, which are known to be very slow (Gould & Salpeter 1963).

In this paper, we investigate the possibility of gas-phase formation of H_2 mediated by polycyclic aromatic hydrocarbons (PAHs). PAHs are good candidates for several reasons.

1. The detection in the IR of an emission band at 3.3 μm is evidence for the existence of PAHs in the interstellar medium (ISM) because it is the signature of an H atom attached to an aromatic structure. Moreover, the benzene molecule, C_6H_6, has been detected recently in CR618 (Cernicharo et al. 2001). It is thought that PAHs may contain up to 20% of the available carbon in the ISM (Boulanger 1999).
2. It is known that the radiative association between molecules strongly depends on the size of the molecules (Herbst & Dunbar 1991). Comparison of the rate constant for radiative association of $H^+ + H$ which is $< 10^{-18}$ cm^3 s^{-1} and the rate constant for $C_{10}H_7^+ + H_2$ which is 1.2×10^{-11} cm^3 s^{-1} (Snow et al. 1998) indicates that this latter reaction is relatively efficient.
3. H_2 emission correlates with PAH emission (Joblin et al. 2000; Pety et al. 2005). This work can be seen as a preliminary answer to a question raised by Boulanger et al. (2000, p. 215) "The high H_2 formation rate proposed here to account for the H_2 emission temperature does not fit with formation from physisorbed H atoms on grain surfaces which is effective only at low temperatures. It suggests that H_2 formation, at least in photon-dominated regions (PDRs), comes from chemically attached H atoms. One possibility which still needs to be experimentally and/or theoretically validated is the reaction of free H atoms with H atoms attached on the periphery/surface of PAHs."

2. H_2 FORMATION USING RECOMBINATION BETWEEN HYDROGENATED PAH IONS AND ELECTRONS

A few models have been proposed where PAHs catalyze the formation of molecular hydrogen. Most of these mechanisms rely on two distinct sequences: (1) H_2 formation and ejection and (2) regeneration of the PAH catalysts by capture of H atoms (Cassam-Chenai et al. 1994).

For example, Pauzat & Ellinger (2001)and later Hirama et al. (2003) have proposed the following steps:

$$PAH^+ + H \rightarrow PAH^+_{+H} \quad (1a)$$

$$PAH^+_{+H} + H \rightarrow PAH^+ + H_2 \quad (1b)$$

In these and subsequent equations, PAH represents any normally hydrogenated polycyclic aromatic hydrocarbon, the +H subscript represents the compound with an additional hydrogen atom, the −H subscript represents the dehydrogenated species, and the + superscript denotes the cation.

A closely related mechanism has also been proposed (Bauschlicher 1998):

$$\mathrm{PAH}^{+}_{-\mathrm{H}} + \mathrm{H} \rightarrow \mathrm{PAH}^{+} \tag{2a}$$

$$\mathrm{PAH}^{+} + \mathrm{H} \rightarrow \mathrm{PAH}^{+}_{-\mathrm{H}} + \mathrm{H}_2 \tag{2b}$$

During a previous study of the reactivity of PAH ions in the presence of atomic hydrogen (Le Page et al. 1999a, 1999b), we found that "reaction (1b)" is very slow in the case of benzene, naphthalene, and pyrene, and thus it is likely that the process of direct formation of H_2 from hydrogenated PAH ions reacting with H atoms is very slow. For the second mechanism, the rate-limiting step seems to be "reaction (2b)" which might be slighty endothermic for large PAHs. Moreover, small dehydrogenated PAH ions are usually unreactive with hydrogen atoms, and thus the overall efficiency of the process is probably low. The fact that our experimental knowledge of these reactions is limited to the smallest members of the PAH family with sizes up to the coronene molecule does not prevent these reactions from being efficient for larger PAHs (see Section 4.3). However, we found that the chemistry of PAH ions of different sizes is very similar, and therefore we propose an alternate mechanism based on a reaction network where all reactions were found to be efficient for small PAHs (Le Page et al. 2001, 2003):

$$\mathrm{PAH}_{-\mathrm{H}} + \mathrm{H} \rightarrow \mathrm{PAH} \tag{3a}$$

$$\mathrm{PAH} + h\nu \rightarrow \mathrm{PAH}^{+} + e^{-} \tag{3b}$$

$$\mathrm{PAH}^{+} + \mathrm{H} \rightarrow \mathrm{PAH}^{+}_{+\mathrm{H}} \tag{3c}$$

$$\begin{array}{lc} & \text{Branching ratio} \\ \mathrm{PAH}^{+}_{+\mathrm{H}} + e^{-} \rightarrow \mathrm{PAH}_{+\mathrm{H}} + h\nu & 0 \\ \rightarrow \mathrm{PAH}_{-\mathrm{H}} + \mathrm{H}_2 & a \\ \rightarrow \mathrm{PAH} + \mathrm{H} & 1 - a. \end{array} \tag{3d}$$

The advantage of this framework is that most of these reactions have been studied experimentally—at least for small PAHs—and it is thus possible to estimate numerically the efficiency of this cycle. The least studied reaction is (3a) which has been examined only in the case of benzene (i.e., C_6H_5 + H → C_6H_6) and is expected to proceed with a large rate constant (Mebel et al. 2001). We note that this reaction is a simple radical–radical recombination, and therefore it is not expected to have an activation barrier for larger PAHs. Moreover, this reaction is thought to be increasingly efficient as the PAH size increases, because radiative association processes are size-dependent reactions.

The rates of the other reactions in this mechanism can be estimated using experimental data on small PAHs and our previous model on the reactivity of larger PAHs in the diffuse ISM. "Reaction (3d)" can lead to different products with a branching ratio associated with each channel. The branching ratio reflects the probability for the complex to dissociate through a specific pathway. The reaction can be modeled with Rice–Ramsperger–Kassel–Marcus (RRKM) theory using the framework developed in Le Page et al. (2001); reaction (3b) is estimated using absorption cross sections from Joblin (1992) and the yield toward ionization from the work of Verstraete et al. (1990); finally, the rate of process (3c) is estimated using our previous measurements on the reactivity of small PAH ions.

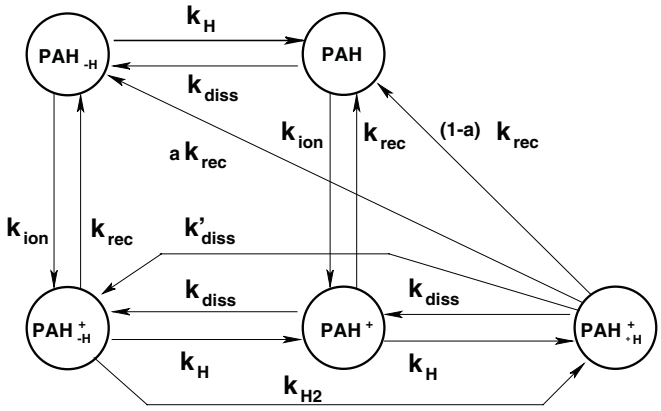

Figure 1. Chemical mechanism used in our computation of H_2 formation. PAH represents any normally hydrogenated PAH (e.g., coronene $C_{24}H_{12}$, ovalene $C_{32}H_{14}$); PAH_{-H} represents the dehydrogenated species where one peripheral hydrogen is missing, while PAH_{+H} represents a PAH with an additional hydrogen atom (e.g., $C_{32}H_{15}$ for ovalene). The + superscript denotes the corresponding cation. Anion chemistry is not included for simplicity. The arrows represent the various processes that transform one PAH into another. Four main processes are considered: (1) ionization with rate constant k_{ion}; (2) recombination between ions and electrons with rate constant k_{rec} and branching ratio a and $(1-a)$ toward H_2 and H formation, respectively; (3) photodissociation with H atom ejection (k_{diss}) or H_2 ejection (k'_{diss}); (4) chemistry with H and H_2 addition through radiative association (k_{H} and k_{H2}).

While the recombination of PAH^+ with electrons can be non-dissociative for PAHs bearing 30 or even 20 carbon atoms it is likely that the recombination of PAH^+_{+H} is highly dissociative due to the low binding energy of the two H atoms bonded to the same carbon atom. In our previous study, we found that the recombination is expected to be dissociative for PAHs bearing up to 200 carbon atoms. Therefore, we assign a branching ratio of 0 to the stabilization channel. As the binding energy of H_2 (4.5 eV) is close to the CH bond energy in a normal PAH (4.8 eV), the branching ratio for the H and H_2 ejection channels may have similar values and we thus assume a branching ratio of 0.5 for both channels.

3. MODEL

In order to assess the overall efficiency of this mechanism in producing H_2 molecules, we can model the process as in Figure 1 where a few minor reactions have been included to enhance the precision.

To estimate the overall efficiency of this mechanism, we need to know the amount of carbon that is locked in PAHs in the ISM and also the distribution of PAH sizes. We then compare the rate of H_2 formation to the rate of H_2 photodissociation. In a steady-state limit in 1 cm^3 of a diffuse cloud, the following equation applies:

$$d[\mathrm{H}_2]/dt = \text{rate of } \mathrm{H}_2 \text{ photodissociation} + \text{rate of } \mathrm{H}_2 \text{ production}.$$

Therefore, at equilibrium,

$$ß_0 n_{\mathrm{H}_2} = R\, n_t\, n_{\mathrm{H}},$$

where $ß_0$ is the unshielded rate coefficient of H_2 photodissociation in a standard UV field, R is the rate coefficient of H_2 formation (from PAHs, grains, and any other source), n_t is the total hydrogen density, and n_{H} and n_{H_2} are the H and H_2 densities, respectively. Note that we do not include dust extinction and that we assume that the UV flux χ in units of Draine's field

Table 1
Rate Coefficient of H_2 Formation Computed for PAHs Having Different Sizes in an Environment Where $f = 0.5$, $n_t = 10$ cm^{-3}, $T = 100$ K and $\chi = 1$

PAH	$C_{50}H_{20}$	$C_{100}H_{28}$	$C_{200}H_{50}$
R_{PAH} (cm^3 s^{-1})	2.1×10^{-17}	1.3×10^{-17}	2.9×10^{-18}

Note. Medium-sized PAHs appear to be better catalysts of molecular hydrogen formation.

is equal to 1. This is equivalent to placing the PAHs on the fringe of the cloud.

The standard unshielded value of β_0 is 5×10^{-11} s^{-1} (Duley & Williams 1984) and the corresponding rate coefficient of H_2 formation to achieve equilibrium has been estimated (e.g., Jura 1975) to be about 3×10^{-17} cm^3 s^{-1} in typical diffuse clouds.

In order to estimate the efficiency of H_2 production using PAHs, we compare our inferred rate coefficient R_{PAH} to this standard value of 3×10^{-17} cm^3 s^{-1}. R_{PAH} will depend on the PAH size, so we have calculated this rate coefficient for different PAHs (e.g., C_{50}, C_{100}, C_{200}). In our network and for a given PAH, the steady-state rate coefficient is equal to

$$R_{PAH} = (a\, k_{rec} n_e + k'_{diss})\, n_{PAH^+_{+H}} / n_t\, n_H,$$

where a is the branching ratio for H_2 production during the recombination process, k_{rec} is the rate constant for recombination of $PAH^+{}_{+H}$ with electrons, n_e is the electron density, k'_{diss} is the rate constant for photodissociation of $PAH^+{}_{+H}$ with H_2 ejection, and $n_{PAH^+_{+H}}$ is the density of $PAH^+{}_{+H}$ which can be estimated using the framework that we have developed (Le Page et al. 2001). For simplicity, the same branching ratio a is used for excited neutral PAH and photoexcited PAH^+ as the mechanisms can be quite similar for large molecules if intramolecular vibrational redistribution (IVR) of energy is efficient. Alternatively, if IVR is not efficient the rate would be even higher, and thus the effect of this assumption is to lower the actual rate. A more crude assumption is to choose a value for the branching ratio a. In most calculations, we assume that H and H_2 ejection are comparable processes in terms of energy, thus leading to a value of 0.5 for a. Only precise quantum calculations or experiments can determine this value.

Boulanger (1999) has estimated the fraction of carbon in PAHs to be about 20% of the solar abundance (70 ppm of the total hydrogen density). Here we take 15% of the estimated average ISM abundance (Snow & Witt 1995), i.e., 0.15×220 ppm $= 33$ ppm, with respect to the total hydrogen density.

We also assume that hydrogen is mostly atomic, $f = 2n_{H_2}/(n_H + 2\, n_{H_2}) \sim 0$–$0.5$; in the fringe of the cloud to which Jura's data refer to, $f \sim 0$. The rates for the different physical processes (e.g., rate of reaction with H, photodissociation, recombination between ions and electrons, etc.) are the same as those inferred in Le Page et al. (2001). The framework of the model is the same as the one described in Le Page et al. (2001); current computations were performed using Scilab 4[3].

4. RESULTS

The results of our model are presented in Table 1 and Figure 2. From this table it appears that medium-sized PAHs are more efficient than large PAHs in producing H_2. This arises primarily from the fact that large PAHs consume more carbon per PAH

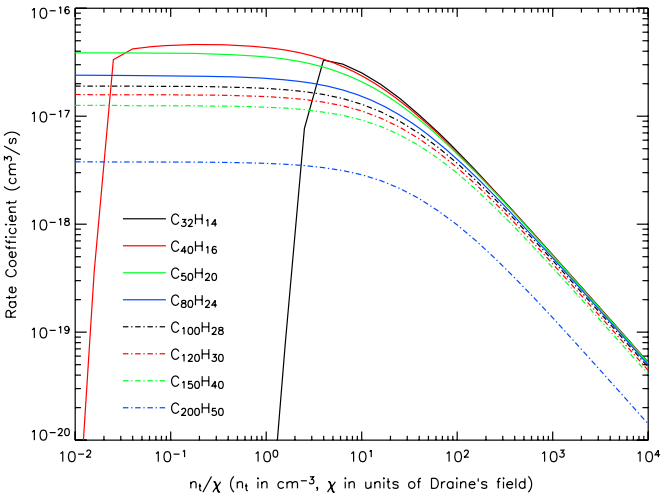

Figure 2. Rate coefficient of H_2 formation for PAHs of different size depending on the ratio n_t/χ of total hydrogen density to UV field intensity in units of Draine. The factor $f = 2n_{H_2}/n_t$ is chosen to be equal to 0.5 and the temperature is set to 100 K. These two factors were found not to be critical and changing them does not significantly alter the shape of the curves.

unit; in addition, in the case of $C_{50}H_{20}$ there is an important contribution of the $PAH^+{}_{+H}$ photodissociation channel ($C_{50}H_{21}{}^+ + h\nu \rightarrow C_{50}H_{19}{}^+ + H_2$, with the rate constant k'_{diss}). It is probable that the density of smaller PAHs is higher than the density of larger PAHs. For example, Tielens (1993) has estimated that the PAH distribution fits well with an extension of the Mathis, Rumpl, & Nordsieck (MRN) distribution (Mathis et al. 1977). If so, medium-sized PAHs will strongly dominate the distribution, and the rate coefficient of H_2 formation will be close to the one derived from $C_{50}H_{20}$. In Figure 2, it appears that the $C_{200}H_{50}$ curve is at a somewhat lower position than the simple $1/x$ ratio would predict (where x is the number of carbon atoms in the PAH). This is due to the fact that, with our model parameters, 60% of the $C_{200}H_n$ molecules are multiply hydrogenated ($n > 51$). While we have not taken into account the possibility of H_2 production by the recombination of multiply hydrogenated PAH ions, it is likely that they contribute with equal yields as the normally hydrogenated PAH through similar processes (i.e., $C_{200}H_n{}^+ + e^- \rightarrow C_{200}H_{(n-2)} + H_2$ with $n > 51$). Our calculations in Table 1 have been made under the assumption that all PAHs are identical in each run (e.g., $C_{50}H_{20}$). In order to estimate a rate coefficient more precisely, one should use a PAH size distribution which gives the overall rate in which each PAH individual rate contributes according to the partial density of the individual PAH within the distribution (see Draine and Li 2007; Flagey et al. 2006).

The generic shape of the rate coefficient of H_2 formation with respect to n_t/χ in Figure 2 can be divided into three parts. These three parts are represented in Figure 3 and correspond to three zones:

1. Zone A: a steep decrease at low n_t/χ, the larger the PAH the steeper the curve,
2. Zone B: a flat 'plateau' where the rate coefficient of H_2 formation is almost constant,
3. Zone C: a slow decrease with density at higher density.

The steep decrease at low n_t/χ is due to the photodissociation of PAH. This situation occurs when the atomic hydrogen density is not large enough to replenish the hydrogen coverage of the

[3] http://www.scilab.org

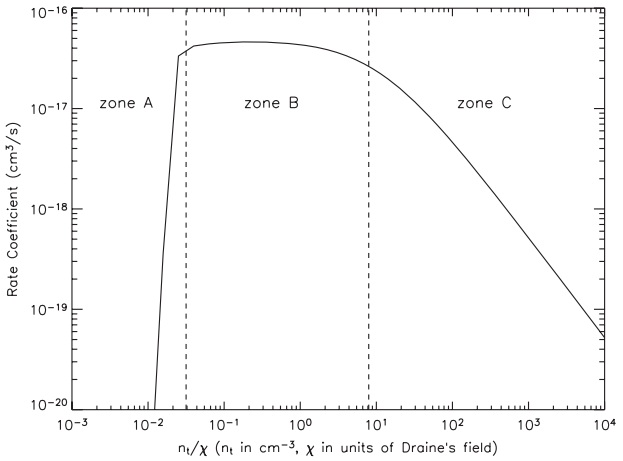

Figure 3. Three different parts of the set of curves shown in Figure 2. Zone A corresponds to harsh environments where the PAH is prone to photodissociation; zone B represents environments where the PAH is mostly ionized; zone C corresponds to areas where the PAH is mostly neutral, thus reducing the formation of H_2 through ion–atom reactions.

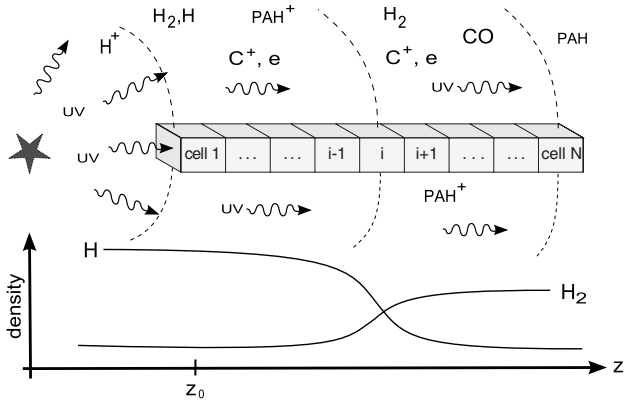

Figure 4. Simple schematic of a PDR. The incoming UV radiation from the star at left ionizes the material and dissociates molecules. When the UV field penetrates further inside the PDR, its intensity decreases and more complex molecules can be built. The dashed envelopes represent the typical transition layers within the PDR, moving from atomic and ionic species at the left to molecular and neutral species at the right at higher extinction. Cells 1–*N* are sections of the PDR aligned with the star, which are sufficiently small for the different parameters to be constant within the cell (UV flux and density of each species). The H_2 density is calculated in each cell from left to right according to the model presented in Section 4.1. The H_2 formation leads to a decrease of UV intensity through molecular absorption as outlined in the graph at the bottom of the figure.

PAH through consecutive H or H_2 addition. This regime is representative of harsh environments such as H II regions. In our model, it is assumed that the UV flux is not large enough to dissociate the carbon skeleton of the PAH because it requires considerably more energy to break the C skeleton than to eject an H or H_2 fragment. In cases of high UV flux, the PAH is almost completely dehydrogenated and the rate coefficient of formation of H_2 is proportional to the fraction of PAH having a normal hydrogen coverage. The hydrogenation is mainly controlled by H_2 addition which in turn will depend on n_H and χ. If f, the ratio $2n_{H_2}/n_t$ of hydrogen locked in a molecular form to the total hydrogen density, remains constant, the curve will have a dependence of the form $(n_t/\chi)^y$ for low f values and $(n_t/\chi)^{(y/2)}$ for environments where H_2 is present. Here y is the normal hydrogen content of a generic PAH, C_xH_y. For example, if a PAH with a normal hydrogen coverage of 10 H atoms is fully dehydrogenated, our mechanism will not be efficient because it requires that the PAH becomes fully hydrogenated before H_2 production can be effective. However, the probability for the PAH to gain one additional H atom is proportional to n_t/χ; hence the probability to become completely hydrogenated is proportional to $(n_t/\chi)^y$ when H is the major species and proportional to $(n_t/\chi)^{(y/2)}$ when hydrogen is mainly molecular. The factor of 1/2 accounts for the fact that hydrogenation through a reaction with molecular hydrogen should be more efficient than with atomic hydrogen.

The largest values of R are obtained on the flat part of the curve. In this area, most PAHs are ionized and bear their normal hydrogen coverage. This environment is representative of diffuse clouds where n_H has a typical value between 1 and 100 cm^{-3}. If we consider that the PAH is fully ionized, the rate coefficient will be close to $1/2\ ak_H\ (C/H)_{PAH}\ /x$, where the branching ratio a is the fraction of $PAH^+{}_{+H}$ leading to H_2 formation when recombining with electrons, $(C/H)_{PAH}$ is the fraction of cosmic carbon locked into PAH, which we choose to be 33×10^{-6} (i.e., 15% of available cosmic carbon), x is the average number of carbons in the PAH, k_H is the rate constant for association of $PAH^+{}_{+H}$ and H, and the factor of 2 takes into account the fact that two hydrogenation steps are required to produce an H_2 molecule. If we choose a value of 0.5 for the branching ratio a, we find that for a typical PAH of 50 carbon atoms, the rate coefficient has a value of 4×10^{-17} cm^3 s^{-1}, in very good agreement with the accepted standard value of 3×10^{-17} cm^3 s^{-1}.

The last part of the curve shows a decrease of R at higher hydrogen density. This situation occurs when the electron recombination rate of PAH is faster than the photoionization rate. The balance between ions and neutrals is displaced toward neutrals when the density increases because the recombination rate is proportional to the electron density, which in turn depends on n_H. The curve is thus expected to have a slope of -1. This part of the curve represents astrophysical environments with higher densities such as translucent clouds and fringes of molecular clouds.

4.1. A Simple Test: The ρ Oph PDR

Located at 140 pc from the Sun (Snow et al. 2008) the ρ Oph main cloud L1688 is illuminated by the B2 star HD147889 on its western edge. This PDR is seen edge-on from Earth and is thus a good target for testing the agreement between PDR models and observations. This PDR has been studied extensively by Habart and co-workers (2003, 2004, 2005) using the ISO-SWS data for PAH emission and ESO observations for the H_2 1–0 S1 emission lines. From these measurements they were able to derive the density and the temperature profile of the PDR. They found a good correlation between PAH emission and H_2 emission; from the results of the model it was concluded that H_2 was likely to be formed on PAHs through chemisorption/ejection at the surface of the molecule and that the H_2 formation rate coefficient was higher than the standard value of 3×10^{-17} cm^3 s^{-1} found in the diffuse ISM.

The ρ Oph PDR offers a good example for testing the ability of our model to produce H_2 in a known environment. Using the values found by Habart and coworkers, namely the temperature, the total density, the ratio of carbon locked in PAH, and the UV flux, it is possible to run the model to see how the column density of molecular hydrogen is built from the edge of the PDR where the hydrogen is mostly atomic, up to the molecular cloud where the hydrogen is molecular. This allows us to estimate the width of the H/H_2 transition layer and to compare it to the

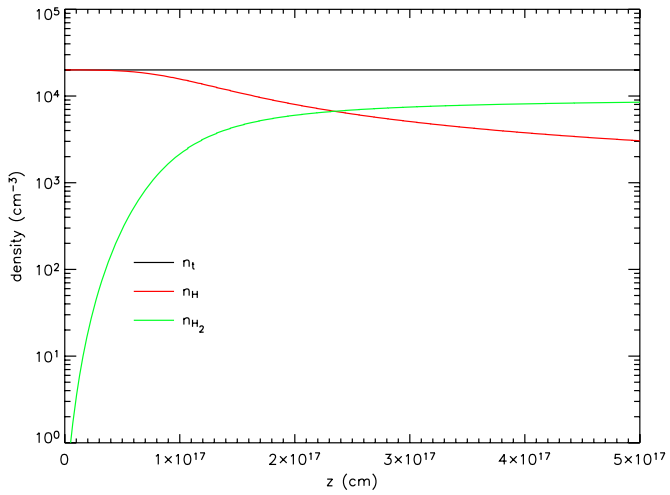

Figure 5. Result of a simple model of forming H_2 in a PDR. The H/H_2 transition layer is thin (about 0.05–0.1 pc) and shows that the model is efficient in producing H_2 despite the strong UV field.

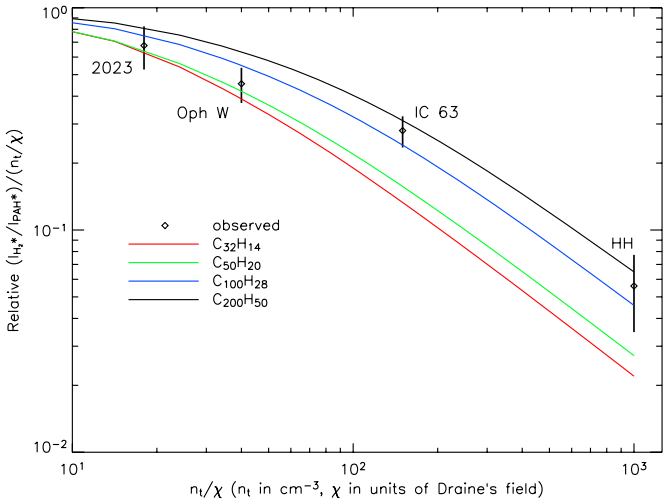

Figure 6. Comparison between observation and the prediction of the model. The general trend of the lowering of the ratio at higher values of n_t/χ is well followed by the model. The Orion bar data have been used to scale the other observed data to produce relative values. The values for R are calculated in the fringe of the cloud as in Figure 2. The effect of dust extinction has not been included as discussed in Section 4.1. Error bars are from Habart et al. (2004), except for the Horsehead Nebula (Habart et al. 2005).

observation. This represents a good test of the overall efficiency of our model in H_2 production.

Figure 4 shows a simple schematic of a PDR that is divided into cells from 1 through N. $\beta_{H_2}(i)$, the coefficient of self-shielding of H_2, is first computed using the integral H_2 column density between the star and the current cell i where the calculation is performed:

$$\beta_{H_2}(i) = F[N_{H_2}(i-1)].$$

The ratio $f = 2n_{H_2}(i-1)/n_t$ is also computed in order to calculate the rate coefficient of hydrogen formation R:

$$R(i) = R(i, f, n_t, \text{env}),$$

where env represents all other environmental variables such as T, n_e, χ, and all rate constants such as k_{rec}, k_H as described in Figure 1.

Knowing $R(i)$ and $\beta_{H_2}(i)$, it is possible to calculate the molecular hydrogen density $n_{H_2}(i)$ in the cell i:

$$n_{H_2}(i) = \frac{n_t}{2 + \frac{\chi\,\beta_{H_2}(i)}{R(i)n_t}},$$

which in turn allows us to calculate the H_2 column density between the star and cell i:

$$N_{H_2}(i) = N_{H_2}(i-1) + n_{H_2}(i)\,dz,$$

where dz is the longitudinal width of cell i in cm.

With the computed value of N_{H_2} in cell i it is possible to continue the calculation on cell $i+1$ up to the edge of the PDR. The effect of dust extinction is rather small in this case because the PDR has a n_t/χ ratio of about 40, and thus lies in zone C in Figure 3 where the rate coefficient of H_2 production shows a slope of -1 in its dependence on n_t/χ. In this zone, the effect of dust extinction is twofold: (1) the dust extinction lowers the amount of UV available to produce PAH^+ and thus lowers the rate coefficient of H_2 production by the same amount. (2) The dust extinction better shields H_2 and prevents photodissociation as there are fewer high-energy photons available. The net result is that the inclusion of dust does not significantly change the H_2 column density.

The results for $n_{H_2}(z)$ are presented in Figure 5. The following values were used for the main parameters: $T = 300$ K, $n_t = 2 \times 10^4$ cm^{-3}, $(C/H)_{PAH} = 7.5 \times 10^{-5}$, and $\chi = 400$; the dependence between n_{H_2} and the self-shielding of H_2 was found in Duley and Williams (1984). The dependence of β_{H_2} on N_{H_2} is modeled as a straight line in log–log scale going from 5×10^{-11} s^{-1} for $N_{H_2} = 1 \times 10^{15}$ cm^{-2} to $\beta_{H_2} = 6 \times 10^{-15}$ s^{-1} for $N_{H_2} = 1 \times 10^{20}$ cm^{-2}. A cutoff value of 5×10^{-11} s^{-1} is assumed for column densities smaller than 1×10^{15} cm^{-2}. As can be seen, the model is very effective in producing H_2, and the H/H_2 transition layer is about 0.05 pc wide in agreement with the observations.

4.2. Comparison with Observations

The ratio of emission of excited molecular hydrogen H_2^* to emission of PAH^* molecules can be expressed as

$$q = \frac{I_{H_2^*}}{I_{PAH^*}} \propto \frac{\text{number of excited } H_2^* \text{ molecules per volume}}{\text{number of excited } PAH^* \text{ molecules per volume}}.$$

The numerator is proportional to $Rn_H n_t$ while the denominator is proportional to the density of PAH, which in turn is proportional to n_t if we make the reasonable assumption that the ratio $(C/H)_{PAH}$ of carbon locked into PAH molecules is approximately constant in the ISM. Hence we have

$$q \propto \frac{Rn_H}{\chi}.$$

We thus expect $q/(n_t/\chi)$ to be proportional to R; we note that Habart et al. (2004) have discussed this relationship for their model that includes dust extinction. Table 2 shows the value of $q/(n_t/\chi)$ for five PDRs covering a large range of n_t/χ values. The data are plotted in Figure 6 together with a fit for different PAH sizes. The best fit is obtained for a size of about 100 carbon atoms. The decrease of R for large values of n_t/χ depends mainly on the competition between ionization and electron recombination as discussed in Section 4.1.

The estimation of PAH size cannot be better than the accuracy to which rates of both ionization and recombination are known.

Table 2
Environmental Parameters for Several PDRs and the Ratio of the Intensity of Vibrationally Excited H_2 Emission to the Intensity of Emission by Excited PAH in the IR Region

PDR	Orion bar[a]	NGC 2023[a]	Oph W[a,b]	IC 63[a]	Horsehead[c]
$I_{H_2^*}/I_{PAH^*}$	0.0003	0.0009	0.0013	0.003	0.004
n_t/χ	4.2	18	40	150	1000

Notes.
[a] Habart et al. (2004).
[b] Habart et al. (2003).
[c] Habart et al. (2005).

Another source of error is the collisional quenching of the excited molecular hydrogen in regions of higher density. In the case of the Horsehead Nebula, it is likely that half of the excited H_2 is quenched by the surrounding gas which leads to an underestimation of the rate and of the mean PAH size (see Appendix A1.4 of Sternberg & Dalgarno 1995).

There are too many uncertainties in recombination rates of PAHs with electrons and in the C/H ratio attributed to PAHs to draw firm conclusions. However, while not quantitative, Figure 6 shows that our model reproduces well the trend of smaller R at higher n_t/χ ratios because the decrease of the ratio q can easily be explained at large n_t/χ values if only PAH ions contribute to the formation of H_2^* as assumed in our model. This is not specific to this model and the same behavior can be inferred from other models where H_2 is formed by PAH ions, as in the proposals of Pauzat, Bauschlicher, or Hirama. The rate of ionization is known to scale with the total number of carbon atoms with reasonable agreement but very little is known about the rate of recombination with electrons for larger PAHs. Recent results show a positive dependence of the rate of recombination on PAH size (Novotny et al. 2005; Biennier et al. 2006); the rate of recombination between the pyrene ion and an electron approaches the value deduced from an extension of classical grain theory toward the smallest sizes. Therefore, we have chosen this rate, following in this case the choice of Vuong and Foing (2000). Experimental values of the recombination of PAH ions larger than pyrene with electrons are thus needed to investigate this point further.

The fact that there is a good correlation between the emission of PAHs (between 5 and 8.5 μm) and the H_2 emission supports this model. Moreover, the decrease in H_2 emission was found to be correlated with the decrease of the UV field intensity (see Figure 3 in Boulanger et al. 2000); this observation is more readily explained by the present model (see zone C of Figure 3 where the decrease of R is inversely proportional to the increase of χ) than by a conventional grain model.

4.3. Variations of Parameters

If we change the rates of the various processes involved in this mechanism, it is possible to achieve higher rates of H_2 formation. Although there are many independent rates in this model it appears that only a few are critical. The reason is that the PAHs are used as catalysts and are not consumed in the model; thus the entire process can be viewed as a cycle whose overall rate is determined by the rate of the slowest processes. In our cycle, the rate-limiting steps are the rates of association of $PAH^+{}_{-H}$ and PAH^+ with H, and the branching ratio a. For the two rate constants we have taken values of 1.6×10^{-10} cm^3 s^{-1} and 2×10^{-10} cm^3 s^{-1}, respectively, based on measurements carried out on small PAH ions. If we assume Langevin rates (i.e., every collision is reactive) for these processes an H_2 production rate coefficient $> 10^{-16}$ cm^3 s^{-1} can be achieved. The variation of the rate with the size of PAH ions is also important, especially for reactions with atoms.

From a simple particle-in-a-box argument, it is evident that the increase of PAH size will lead to a general lowering of the energy difference between electronic levels in the PAH molecule because the energy spacing between molecular levels decreases when the PAH size increases. This can lead to the opening of channels that are not available for smaller PAHs because the ion–molecule chemistry is governed by the relative position of energy levels in the molecular reactants and products. For example, large doublet PAH ions may react with ground-state doublet atomic hydrogen to form a product in a triplet state if the singlet–triplet splitting of the product is small enough (i.e., the energy difference between the ground singlet state and the first excited triplet state). This can lead to the interesting possibility of chemiluminescence of large PAH ions in the IR if intersystem crossing is not the dominant process of energy redistribution. This mechanism merits further investigation theoretically and experimentally for possible connection with the Extended Red Emission (ERE) seen in many different astrophysical environments (Witt and Vijh 2003); this mechanism can naturally explain the absence of emission in the visible region, which has been a major objection for PAHs being the carriers of the ERE. Under this assumption the absence of visible emission arises simply from the fact that the reaction is not sufficiently exothermic to populate levels associated with transitions in the visible spectrum.

5. CONCLUSIONS

The chemistry of small polyatomic molecules suffers from very low radiative association rates, which impedes the buildup of complexity in the ISM. In grains, most of the molecular constituents are buried below the surface and thus cannot participate in the gas-phase chemistry. Intermediate in size between the small polyatomics and small grains, PAHs represent a class of molecules with a good compromise between reactivity and stability. This unique balance makes them efficient chemical agents even at low density.

The proposed model of H_2 formation as a product of the recombination of hydrogenated PAH ions with electrons exemplifies the potential richness of this class of molecules. This mechanism appears to be sufficiently effective to produce molecular hydrogen with a rate coefficient which is comparable to that inferred in standard models of astrochemistry.

This work has been supported by the National Aeronautics and Space Administration. We are thankful to Joshua Destree for help in figure preparation and formatting. We appreciate the helpful comments of an anonymous reviewer.

REFERENCES

Bauschlicher, C. W. 1998, ApJ, 509, L125
Biennier, L., Alsayed-Ali, M., Foutel-Richard, A., Novotny, O., Carles, S., Rebrion-Rowe, C., & Rowe, B. 2006, Faraday Discuss., 133, 289
Boulanger, F. 1999, in Solid State Matter: The ISO Revolution, Lecture 2, ed. L. d'Hendecourt, C. Joblin, & A. Jones (New York: Springer), 19
Boulanger, F., Habart, E., Abergel, A., Falgarone, E., Pineau des Forêts, G., & Verstraete, L. 2000, in Molecular Hydrogen in Space, ed. F. Combes & G. Pineau des Forêts (Cambridge: Cambridge Univ. Press), 211
Cassam-Chenai, P., Pauzat, F., & Ellinger, Y. 1994, in Molecules and Grains in Space, ed. I. Nenner (Woodbury, NY: AIP), 543
Cernicharo, J., Heras, A. M., Tielens, A. G. G. M., Pardo, J. R., Herpin, F., Guélin, M., & Waters, L. B. F. 2001, ApJ, 546, L123

Draine, B. T., & Li, A. 2007, ApJ, 657, 810
Duley, W. W., & Williams, D. A. 1984, Interstellar Chemistry (New York: Academic)
Flagey, N., Boulanger, F., Verstraete, L., Miville Deschênes, M. A., Noriega Crespo, A., & Reach, W. T. 2006, A&A, 453, 969
Gould, R. J., & Salpeter, E. E. 1963, ApJ, 138, 393
Habart, E., Abergel, A., Walmsley, C. M., Teyssier, D., & Pety, J. 2005, A&A, 437, 177
Habart, E., Boulanger, F., Verstraete, L., Pineau des Forêts, G., Falgarone, E., & Abergel, A. 2003, A&A, 397, 623
Habart, E., Boulanger, F., Verstraete, L., Walmsley, C. M., & Pineau des Forêts, G. 2004, A&A, 414, 531
Herbst, E., & Dunbar, R. C. 1991, MNRAS, 253, 341
Hirama, M., Ishida, T., & Aihara, J-I 2003, Comput. Chem., 24, 1378
Joblin, C. 1992, PhD thesis, Univ. of Paris
Joblin, C., Maillard, J. P., Vauglin, I., Pech, C., & Boissel, P. 2000, in Molecular Hydrogen in Space, ed. F. Combes & G. Pineau des Forêts (Cambridge: Cambridge Univ. Press), 107
Jura, M. 1975, ApJ, 197, 575
Le Page, V., Keheyan, Y., Bierbaum, V. M., & Snow, T. P. 1999a, J. Am. Chem. Soc., 121, 9435
Le Page, V., Keheyan, Y., Snow, T. P., & Bierbaum, V. M. 1999b, Int. J. Mass Spectrom., 185, 949
Le Page, V., Snow, T. P., & Bierbaum, V. M. 2001, ApJS, 132, 233
Le Page, V., Snow, T. P., & Bierbaum, V. M. 2003, ApJ, 584, 316
Mathis, J. S., Rumpl, W., & Nordsieck, K. H. 1977, ApJ, 217, 425
Mebel, A. M., Lin, M. C., Chakraborty, D., Park, J., Lin, S. H., & Lee, Y. T. 2001, J. Chem. Phys., 114, 8421
Novotny, O., Sivaraman, B., Rebrion-Rowe, C., Travers, D., Biennier, L., Mitchell, J. B., & Rowe, B. R. 2005, J. Chem. Phys., 123, 104303
Pauzat, F., & Ellinger, Y. 2001, MNRAS, 324, 355
Pety, J., Teyssier, D., Fossé, D., Gérin, M., Roueff, E., Abergel, A., Habart, E., & Cernicharo, J. 2005, A&A, 435, 885
Snow, T. P., Destree, J. D., & Welty, D. E. 2008, ApJ, 679, 512
Snow, T. P., Le Page, V., Keheyan, Y., & Bierbaum, V. M. 1998, Nature, 391, 259
Snow, T. P., & Witt, A. N. 1995, Science, 270, 1455
Sternberg, A., & Dalgarno, A. 1995, ApJ, 99, 565
Tielens, A. G. G. M. 1993, in Dust and Chemistry in Astronomy, ed. T. J. Millar & D. A. Williams (Bristol: Institute of Physics Publishing), 103
Verstraete, L., Léger, A., d'Hendecourt, L., Dutuit, O., & Défourneau, D. 1990, A&A, 237, 436
Vuong, M. H., & Foing, B. H. 2000, A&A, 363, L5
Witt, A. N., & Vijh, U. P. 2004, in ASP Conf. Ser. 309, Astrophysics of Dust, ed. A. N. Witt, G. C. Clayton, & B. T. Draine (San Francisco, CA: ASP), 115